DOI: 10.1002/ejic.201001071

Vertically Well-Aligned In_2O_3 Cone-Like Nanowire Arrays Grown on Indium Substrates

Wenyan Yin,[a] Matt Doty,[b] Chaoying Ni,[b] Changwen Hu,*[a] Minhua Cao,*[a] and Bingqing Wei*[c]

Keywords: Indium / Nanostructures / Chemical vapor deposition / Arrays / Luminescence

Single-crystalline, cone-like In_2O_3 nanowire (NW) arrays were directly synthesized on the surface of indium grains without any catalyst by using a simple chemical vapor deposition (CVD) method. The indium grains served both as the indium source, which reacted with different oxygen sources, and the substrate for the growth of the cone-like In_2O_3 NW arrays. The controllable synthesis of the cone-like In_2O_3 NW arrays with variable densities, sizes, and morphologies were achieved by adjusting the oxygen sources. A possible mechanism was proposed for the formation of the cone-like In_2O_3 NW arrays. The photoluminescence spectrum of the low-density, cone-like In_2O_3 NW arrays shows emission in a wide range, from the visible (yellow light) into the near infrared region.

1. Introduction

One-dimensional (1D) semiconductor nanowires (NWs) have become the focus of intensive investigations over the past decade for a variety of applications such as optoelectronic devices and sensors.[1–3] So far, light-emitting diodes,[4] lasers,[5] photodetectors,[6] and field-effect transistors[7,8] have been made from these semiconductor NWs. Among them, vertically oriented 1D NWs are the basic building blocks for constructing such devices and are particularly interesting. Different 1D NW arrays can be formed through self-assembly of these basic NW building blocks. Compared with randomly distributed NWs reported in earlier studies, vertically oriented semiconductor NW arrays with controllable diameter and length are likely more suitable for many applications, such as solar cells, active elements for 3D electronics.[9–11] In view of the increasing interest in 1D NW arrays, it is of great importance to design and synthesize them in order to study their potential technological applications. At the same time, understanding the growth mechanisms and key growth processes is of critical importance and remains a challenge for control and optimization of the synthesis and properties of NW arrays.

Indium oxide (In_2O_3), a well-known n-type semiconductor oxide with a wide band gap of about 3.6 eV, has been frequently used in the microelectronic field in gas detectors, window heaters, solar cells, memory devices, and flat-panel display materials.[12–14] Almost all of the reported In_2O_3 nanomaterials, particularly In_2O_3 NWs,[15–18] have been prepared by well-developed methods such as chemical vapor deposition (CVD),[15,16] pulsed laser deposition (PLD),[17] alumina or mesoporous silica template method,[18] and so on. However, to the best of our knowledge, current methods reported for the synthesis of oriented 1D In_2O_3 NW arrays generally suffer from some drawbacks, such as costly substrates, catalysts, metalorganic precursors, and inexpungible templates.[18–22] Therefore, there is a need to synthesize controllable In_2O_3 NW arrays through other facile, economical, effective approaches on simple substrates without catalysts, rigorous vacuum conditions, and complicated templates.

In the study reported in this paper, cone-like In_2O_3 NW arrays were grown in situ on the surface of indium grains at 900 °C by a simple CVD route. Here, the indium grains served themselves as both the indium source, which reacted with different oxygen sources, and as the substrate for the growth of cone-like NW arrays. Cone-like In_2O_3 NW arrays with controllable densities, sizes, and morphologies were achieved by adjusting the oxygen sources. The mixture of gallium oxide and graphite powder or industrial purity argon with a trace amount of oxygen (2 ppm) acted as the different oxygen sources. The low-density, well-aligned, cone-like In_2O_3 NW arrays were obtained when the mixture of gallium oxide and graphite powder acted as the oxygen source. When the industrial purity argon acted as a carrier gas and oxygen source, high-density cone-like In_2O_3 NW arrays were obtained, in which the cones have a nanometer-

[a] Key Laboratory of Cluster Science, Ministry of Education of China, Department of Chemistry, Beijing Institute of Technology,
Beijing 100081, P. R. China
E-mail: caomh@bit.edu.cn
cwhu@bit.edu.cn
[b] Department of Materials Science and Engineering, University of Delaware,
Newark, DE 19716, USA
[c] Department of Mechanical Engineering, University of Delaware,
Newark, DE 19716, USA
E-mail: weib@udel.edu

sized tip and a micrometer-sized root. Compared with the reported methods mentioned above, this method has some distinctive advantages, such as controllable products, a catalyst-free, environmentally benign precursor, and mild reaction conditions. A possible mechanism was proposed for the formation of the cone-like In_2O_3 NW arrays. Furthermore, it is found that the low-density cone-like In_2O_3 NW arrays show a unique photoluminescence emission spectrum spanning the region from the visible (620 nm) to infrared range (800 to 948 nm). This is the first report of infrared emission from nanosized In_2O_3. The unique photoluminescence properties of these In_2O_3 cone-like NW arrays provide many advantages over conventional emitters in the UV/Vis region. The use of laser diodes for excitation and photodiodes for detection makes near-infrared fluorophores an ideal choice as tracers for various applications in commercial (remote devices, infrared connections for mobile telephones), industrial, military (telescopes), biological (decreasing autofluorescence and the sensitivity of detection), and medical phototherapy fields.

2. Results and Discussion

2.1. XRD Pattern and Raman Spectrum

The crystal structure of the samples has been identified by XRD. Figure 1a shows a typical XRD pattern of the low-density cone-like In_2O_3 NW arrays obtained on the surface of indium grain at 900 °C for 1 h. All the diffraction peaks can be indexed well as a body-centered cubic crystal phase [space group: Ia_3 (206)] In_2O_3 (JCPDS No: 06-0416). No other impurity phase, such as pure In, was detected, revealing the phase purity of the In_2O_3 cone-like NW arrays. To further investigate the structure and local atomic arrangement of the as-synthesized In_2O_3 NW arrays, Raman scattering measurements were carried out. Figure 1b displays the room-temperature Raman-scattering spectrum of the In_2O_3 cone-like NW arrays. In the range 100–700 cm^{-1}, six peaks centered at 108, 131, 306, 364, 494, and 629 cm^{-1} can be ascribed to body-centered cubic In_2O_3.[23,24] This agreement between XRD and Raman results indicates that the obtained In_2O_3 NWs in the range 250–320 nm in diameter are stable in the pure cubic phase structure without any phase transformation.

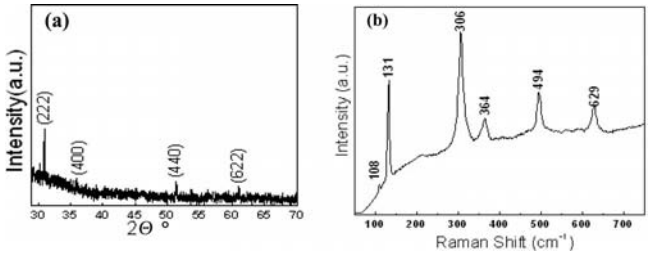

Figure 1. (a) XRD pattern and (b) Raman spectrum of low-density, cone-like In_2O_3 NW arrays obtained on the surface of indium grain at 900 °C for 1 h.

2.2. Characterization of Morphology, Size, and Microstructure

Figure 2a–c shows the FE-SEM images of the low-density In_2O_3 NW arrays grown on the surface of indium grains with the mixture of gallium oxide and graphite powder as oxygen source at 900 °C for 1 h. It was found that the surface of the grains is almost completely covered with the nanowires, even at the edges of the indium grains. Furthermore, most nanowires of the arrays are perpendicular to the surface of the grain, although the grain surface is not flat. Figure 2a shows the FE-SEM image of In_2O_3 NW arrays grown in the middle of the surface of indium grain. It can be clearly seen that all the NWs have cone-like structures although the surface of the indium grain is not flat, because of the low melting point of indium metal (156.6 °C). The diameter of the top of the cone-like nanowires is around 50 nm and the length varies from 2.0 to 5.0 μm, while the bottom diameter of the In_2O_3 nanowires is estimated to be about 310 nm, and each individual cone consists of a well-faceted stem and head. Figure 2b shows the FE-SEM image of the cone-like In_2O_3 NW arrays grown on the lateral surface of the indium grain. The average length of each cone-like NW is about 8.0 μm, which is much longer than that grown in the middle of the indium grain. However, the bottom diameter of the nanowire is about the same as that of the cone-like NW arrays grown in the middle of the indium grain. As shown in Figure 2a,b, the diameter of the cone-like NWs gradually decreases from the bottom to top to form a sharp tip, which is similar to an arrow-like structure. The separation of the NWs on the surface of the indium substrate is about 1.0 μm. The high-magnification FE-SEM image in Fig-

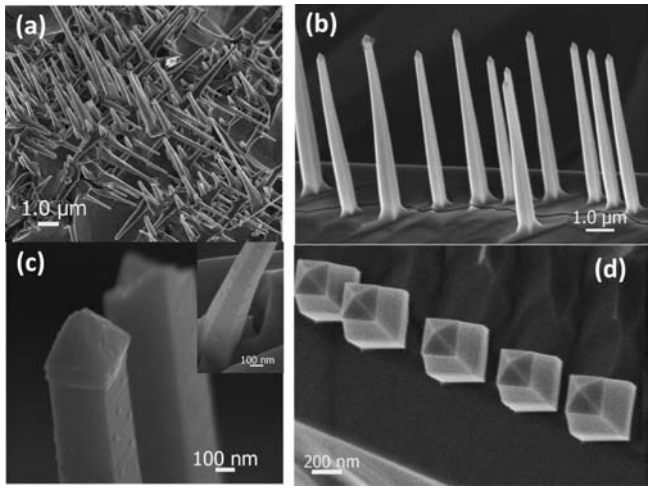

Figure 2. (a) Typical low-magnification FE-SEM image of cone-like In_2O_3 NW arrays grown in the middle of the surface of an indium grain. (b) Typical low-magnification FE-SEM image of cone-like In_2O_3 NW arrays grown on the edge of the surface of an indium grain. High-magnification FE-SEM image of (c) the cone tip, cross-section of the In_2O_3 NWs. The inset in (c) is the base of the cone-like In_2O_3 nanowire. (d) The uniform growth on the surface of the indium and the rectangular footprint of the pyramidal base after heating for 5 min.

ure 2c clearly reveals that the tip of the cone-like nanowires is pyramidal with a rectangular cross-section. An edge of the base of the pyramid is around 210 nm and that of the tip of the pyramid is around 50 nm. Additionally, there are many scattered dots with a diameter of 10 nm on the surface of these stems as shown in Figure 2c. The inset in Figure 2c clearly shows the magnified FE-SEM image of the bottom of the cone-like stem, and the diameter of the stem decreases from the bottom to the tip.

To further study the microstructure of the cone-like In_2O_3 nanowires, TEM analysis was performed. Figure 3a is a low-magnification TEM image of a single cone-like nanowire, which is in agreement with the observation from SEM analysis. Figure 3b shows the corresponding HRTEM image and the selected area electron diffraction (SAED) pattern (inset), both recorded at the tip of the wire. It indicates well-defined lattice fringes with body-centered cubic phase In_2O_3, confirming the single-crystalline nature of the nanowire. Amorphous structure is scarcely seen on the surface. The wire has identical lattice fringes with a *d* spacing of 0.418 nm, which corresponds to the {211} crystal facet. From SAED, the lattice planes of (200) and (211) are indexed. Therefore, the growth direction of the tip of the cone-like wire is along the [211] direction (Figure 3b). Figure 3c is the HRTEM image on the body of the cone-like wire. The lattice plane spacing is also 0.418 nm, corresponding to the lattice plane (211) as well, and the SAED pattern also confirms the single-crystalline nature of the nanowire. Combining the HRTEM of the body of the nanowire with that of the nanowire tip, it can be concluded that the whole nanowire grows along the [211] direction.

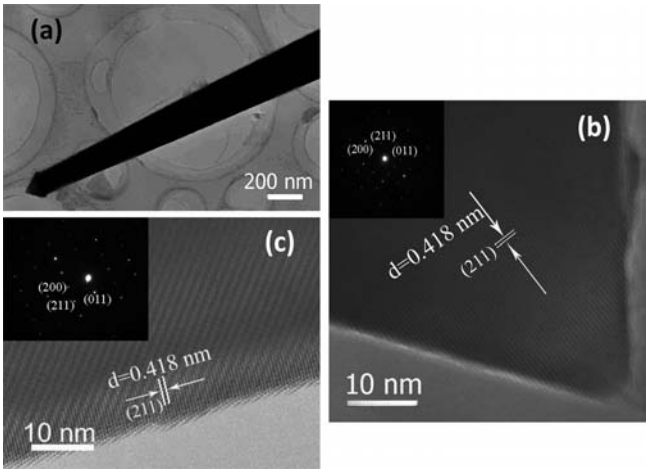

Figure 3. (a) Bright-field TEM image of a typical cone-like NW. (b) HRTEM image taken of the tip of the cone-like wire. The inset in (b) is the SAED pattern of the tip of the cone-like NW. (c) HRTEM image of the body of the cone-like wire. The inset in (c) is the SAED pattern of the body of the wire taken along the [211] zone axis.

It was found that the morphology and the density of the In_2O_3 NW arrays can be controlled by changing the oxygen source. When the mixture of gallium oxide and graphite powder was replaced with industrial grade argon gas with a trace amount of oxygen, while other reaction conditions were kept constant, high-density In_2O_3 NW arrays were obtained. Figure 4a shows a top-view FE-SEM image of uniform In_2O_3 NW arrays over a large area, demonstrating the large-scale, well-aligned, and high-density NW arrays. Figure 4b shows a higher-magnification FE-SEM image, indicating the cone-like, dense NW arrays of the sample. On comparing Figure 4b with the low-density cone-like NW arrays shown in Figure 2a–c, it is interesting to note that the diameter of a single nanowire of the high-density In_2O_3 NWs is also non-uniform, and decreases from the bottom to the top. However, the average length of the NWs is around 70 μm, which is much longer than that of the low-density NWs in Figure 2a–c. Also, between them there is an obvious difference in morphology, which can also be observed in a typical magnified FE-SEM image of a single In_2O_3 nanowire shown in Figure 4c, which indicates a polygon-shaped cross-section with an average diameter of approximately 250–320 nm. It is clearly seen from the inset in Figure 4c that a typical wire consists of a tower-like tip with

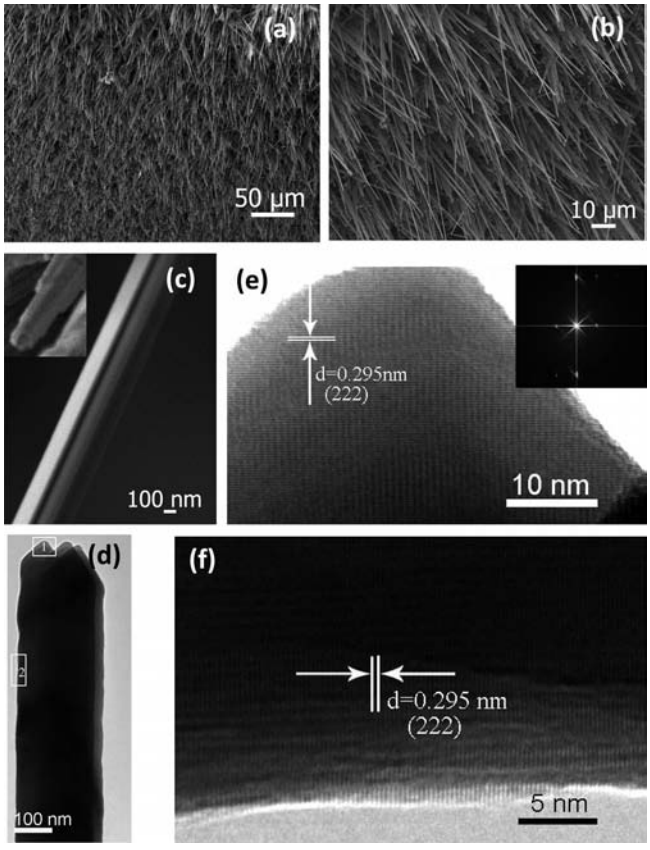

Figure 4. (a) Low-magnification FE-SEM image of high-density In_2O_3 cone-like NW arrays grown on the surface of indium grain. (b) A higher-magnification view of the FE-SEM image in (a). (c) High-magnification FE-SEM image of a part of a single In_2O_3 NW. The inset in (c) is the tip of the cone-like In_2O_3 NW. (d) Low-magnification TEM image of a single In_2O_3 cone-like NW. (e) HRTEM image of the tip of the cone-like wire [white pane 1 in (d)]. The inset in (e) is the FFT pattern on the tip of the wire. (e) HRTEM image of the tip of the cone-like wire. (f) HRTEM image of the body of the cone-like wire [white pane 2 in (d)].

head diameters of 60 nm, which is longer than that of the low-density cone-like NW. The top surface of the tower-like NW is rougher than that of the low-density cone-like NWs. Figure 4d shows a low-magnification TEM image of a single tower-like NW with a diameter of 250 nm. The TEM image further discloses that the tower-like tip of the NW consists of three sharp caps. Figure 4e shows the HRTEM image of the tip (white pane 1 in Figure 4d) of the NW. The lattice spacing is 0.295 nm, which corresponds to {222} crystal planes of the body-centered cubic In_2O_3. The inset in Figure 4e is the corresponding fast Fourier transform (FFT) diffraction pattern of the tip of the NW in Figure 4d, which can be indexed to the single-crystal structure of the individual In_2O_3 tower-like NW. Figure 4f shows a HRTEM image of the body of the In_2O_3 NW (white pane 2 in Figure 4d). The lattice spacing between the adjacent lattice planes perpendicular to the preferential growth direction (marked with arrows) is 0.295 nm, which is consistent with the {222} *d*-spacing of cubic phase In_2O_3, indicating that the NW grows along the [111] direction.

2.3. Formation Mechanism

Although two growth mechanisms exist, namely vapor-liquid-solid (V-L-S)[25] and vapor-solid (V-S),[26] to explain the growth of 1D nanostructures obtained by a gas-phase method, the growth of the cone-like In_2O_3 NW arrays here is inexplicable by these traditional V-L-S and V-S mechanisms. However, on the basis of the experimental results, a possible mechanism is proposed here for the formation of the cone-like In_2O_3 NWs with different densities, morphologies, and sizes. This mechanism consists of four main steps: (I) Fusing (II) Nucleation (III) Primary orientation growth (IV) Surface diffusion growth, as illustrated in Figure 5.

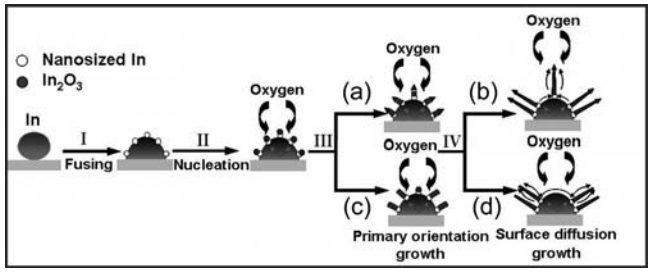

Figure 5. Illustration of a possible growth mechanism of cone-like In_2O_3 NW arrays. (I) Formation of nanosized In droplets during the heating. (II) Reaction of oxygen with In droplets to form In_2O_3 saturation droplets in the nanosized In droplets. (III) Primary growth of In_2O_3 in the nanosized In–In_2O_3 alloy droplets. (IV) Formation of two kinds of In_2O_3 cone-like NW arrays by diffusion of In_2O_3 on the surface of the In grain with sources of oxygen at different concentrations and the final state of In_2O_3 NW arrays.

At elevated temperature, pure indium grain can be easily oxidized to form In_2O_3 molecules by a small quantity of oxygen[27] (we have applied two kinds of oxygen sources as mentioned in the Experimental Section). The first "fusing" stage involves melting of the In grain (melting point of In: 156.6 °C) and the formation of nanosized liquid droplets on the surface of the In grain while heating under an atmosphere containing a small quantity of oxygen, which has been confirmed by the SEM images of the In grains before and after heat treatment. As shown in Figure 6, the original In grain exhibits a relatively smooth surface (Figure 6a), while that after heat treatment displays a rough surface (Figure 6b), which is composed of nanoparticles with an average diameter of 30 nm, denoted as liquid droplets here. The nanosized In liquid droplets not only act as the reactants but also provide an energetically favored sites for oxygen absorption (Figure 5, Step I). Namely, the nanosized In droplets can be seen as "seed templates".

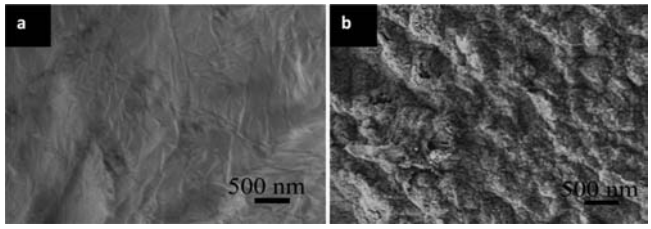

Figure 6. FE-SEM images of the surface of In grain (a) before heating and (b) after heating at 500 °C for 5 min under N_2 flow (heating rate: 10 °C/min).

In the second "Nucleation" stage, the nanosized In "seeds" react rapidly with the oxygen source in the system to yield In_2O_3 nanoclusters on the In droplets to form In–In_2O_3 composite droplets (Figure 5, Step II) at a high temperature of 900 °C. These In_2O_3 nanoclusters initially formed in the In–In_2O_3 droplets are dispersed, and they act as nuclei for the formation of the In_2O_3 NWs when the nanosized In–In_2O_3 droplets reach their saturation concentration. It is believed that the density of the subsequent NW arrays depends on the density of the dispersed In–In_2O_3 droplets.

In the third "Primary orientation growth" stage, the In_2O_3 nucleus in the In_2O_3–In composite droplets reaches the saturation concentration and initiates the growth of the crystalline In_2O_3 NWs [Figure 5, Step III (a–c)]. The In grain directly provides the necessary feeding material (In atoms) for the growth of the In_2O_3 NWs, as indicated by the black arrows in Figure 5.

In the fourth "Surface diffusion growth" stage, as the temperature is maintained constant at 900 °C for 1 h, the NWs continue to grow quickly through the interface of nanosized In_2O_3–In droplets and nanowires by aggregation of molecular In_2O_3 into the In_2O_3–In droplets, resulting in the formation of longer In_2O_3 NWs [Figure 5, Step IV (b,d)]. In addition, in our experiment, in contrast to the smooth surface of indium before heat treatment, the nanosized indium oxide droplets after heat treatment at high temperature have small mismatches with the indium substrate, which is similar to the lattice mismatch reported in ref.[19]

Upon reaching a critical supersaturation concentration, the solvated In_2O_3 molecules crystallize with their (211)/(222) plane heteroepitaxially onto the crystal plane of indium substrate as a result of comparatively minimal lattice mismatch (and hence favorable interfacial surface energy). The small lattice mismatch can be used to explain the growth of NW arrays. However, the morphology of the In_2O_3 appears to be cone-like NWs instead of uniform NWs. To investigate the formation process of the cone-like NWs, time-dependent structure evolution was observed clearly by FE-SEM analysis. Figure 2d shows In_2O_3 grown for 5 min under identical growth conditions as in the 1 h growth (Figure 2a). Some uniform growth of NWs over the surface of the indium grain formed from the rectangular footprint of the pyramidal base can be observed, which means that the In_2O_3 NWs were grown into head cones attached by stem cones eventually. The reason for the formation of the cone-like NWs can be explained according to the proposed growth mechanism below. Similar to the growth of carbon and CN_x tubes by surface diffusion,[27–30] we speculate that, after the "Primary orientation growth" stage, growth by surface diffusion may also be part of the growth process of the In_2O_3 NWs. During the growth of In_2O_3 NWs, the surrounding In_2O_3 molecules were consumed and transported to the tip of In_2O_3 NWs through the surfaces of In grain and In_2O_3 NWs, which nucleated and grew [Figure 5, Step IV(b,d)]. The oxidation reaction of the In grain surface provides In_2O_3 to maintain the surface diffusion and nanowire growth, and thus there is a concentration gradient of In_2O_3 between the bottom and the tip of the In_2O_3 NWs, resulting in a gradual variation of the wire diameter from the root to the tip. Thus, the presence of the concentration gradient results in the formation of the cone-like NWs [Figure 5, Step IV (b,d)]. The indium source is gradually oxidized during diffuse growth, and the tips have a slightly tapered structure along the [211] (Figure 3c) or [222] (Figure 4f) axis. In addition, the surfaces of the cone-like In_2O_3 NWs as shown in Figure 2c have some exiguous nanoparticles, which also support the surface diffusion mechanism. The formation of two kinds of cone-like In_2O_3 NW arrays by diffusion of In_2O_3 on the surface of the In grain can be explained as follows. As we know, surface energies associated with different crystallographic planes are usually different, and they govern the morphology and structure of the crystals.[31] The In_2O_3 nanostructures formed with different growth axes and different cone-like shapes are assumed to be influenced by the surface diffusion on the indium substrate and the surface energy of different In_2O_3 crystal facets. In addition, the oxygen source and the varying concentration and amount of oxygen assist in the formation of the cone-like In_2O_3 NW arrays with two different densities and morphologies in the CVD process. Although the residual air present in the CVD tube may also act as the oxygen source, we hypothesize that the oxygen resource in the reaction system mainly comes from the carbothermal reaction between Ga_2O_3 and graphite powder with a fixed molar ratio of 1:1 as mentioned in the Experimental Section, and the reaction can be summarized as follows:

$$Ga_2O_3\ (s) + 2C\ (s) = Ga_2O\ (g) + 2CO\ (g) \text{ or}$$

$$Ga_2O_3\ (s) + 3C\ (s) = 2Ga\ (g) + 3CO\ (g)$$

Namely, the Ga_2O (g) and the CO (g) are the main oxygen sources and were found to be optimum for the growth of the low-density, cone-like In_2O_3 NW arrays under a 2 L/h N_2 flow rate. To prove this hypothesis, an indium grain without the mixture of Ga_2O_3 and graphite powder was heated at 900 °C for 1 h. A white product covering the surface of the indium grain was characterized with SEM. It was found that the white product mainly consisted of regular polyhedra instead of NW arrays on the surface of the indium grain. If industrial argon with a trace amount of oxygen (δ =2 ppm) acted as the oxygen source, high-density cone-like In_2O_3 NW arrays as shown in Figure 4a,b were observed on the whole edge of the indium grain substrate. It can be concluded that the oxygen concentration has a great effect on the density of In_2O_3 nanocluster nuclei in In–In_2O_3 droplets during the "Nucleation" stage followed by the subsequent growth of the cone-like NW.

2.4. Photoluminescence Properties

It is known that the bulk In_2O_3 does not exhibit photoluminescence (PL) properties at room temperature.[32] However, In_2O_3 nanostructures show PL emission at different wavelengths, indicating that the PL properties of In_2O_3 might be affected by its dimensionality, shape, and size.[33–35] For the low-density cone-like In_2O_3 NW arrays synthesized in our experiment, unique PL peaks were observed in the visible and infrared regions with 390 nm wavelength excitation at room temperature (Figure 7a,b). One stronger wide peak is centered at 620 nm in the orange region, and the other six distinguishable peaks are centered at 800, 808, 836, 871, 908, and 948 nm in the infrared region. This is the first report of infrared emission from nanosized In_2O_3. Generally, oxygen vacancies act as deep defect donors in semiconductors and would induce the formation of new energy levels in the band gap. The 620 nm orange emission was attributed to radiative recombination between an electron on an oxygen vacancy and a hole on an oxygen vacancy center in the In_2O_3 cone-like NW arrays. However, the detailed infrared emission mechanism of the In_2O_3 cone-like NW arrays is not so clear and should be further

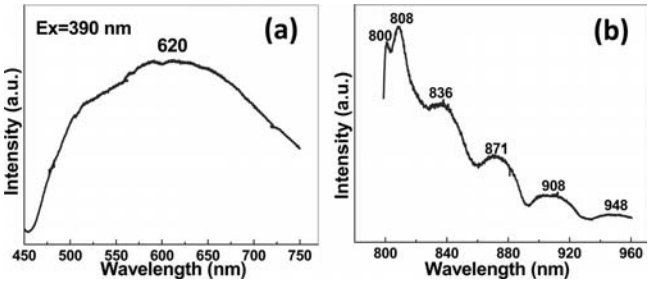

Figure 7. PL emission spectra of low-density In_2O_3 cone-like NW arrays in the (a) visible and (b) infrared range. Excitation wavelength: 390 nm.

studied. The PL properties of the cone-like In_2O_3 NW arrays in a wide visible/infrared range are likely to have potential applications in optoelectronic devices, biological fields and medical phototherapy.

3. Conclusions

New cone-like In_2O_3 NW arrays have been synthesized on the surface of indium grain substrate without any catalyst by using a simple CVD route. The controllable synthesis of the cone-like In_2O_3 NW arrays with different densities, sizes, and morphologies was achieved by simply adjusting the oxygen sources. Mixtures of: (1) gallium oxide and graphite powder, and (2) industrial purity argon with a trace amount of oxygen (2 ppm) acted as the different oxygen sources. A possible formation mechanism of the cone-like In_2O_3 NW arrays was proposed and discussed in detail. The low-density, cone-like In_2O_3 NW arrays exhibit unique photoluminescence properties.

4. Experimental Section

The In_2O_3 cone-like NW arrays were grown in situ on the surface of indium grains with a mixture of gallium oxide and graphite powder as the oxygen source. All experiments were carried out in a tube furnace, similar to the conventional CVD system, as shown schematically in Figure 8. A quartz tube (inner diameter 3.9 cm, length 145 cm) was mounted horizontally inside a tube furnace. High-purity indium grains (purity 99.999%) with 4 mm diameter were horizontally placed downstream from a quartz boat, and the mixture of gallium oxide and graphite powder (Ga_2O_3: graphite = 1:1 molar ratio) was loaded upstream from the quartz boat. The quartz boat was then mounted at the center of the quartz tube. The distance between the mixture powder and the indium grain was about 10 cm. High-purity N_2 carrier gas with a constant flow rate of 2 L/h was initially introduced into the CVD system by the inlet of the tube for 10 min for purging the chamber, and this N_2 flow was then maintained during the whole synthesis process. The furnace was heated up to 900 °C at a heating rate of 10 °C/min and kept at that temperature for 1 h. Low-density, cone-like In_2O_3 NW arrays were obtained on the surface of the indium grains after the CVD system was naturally cooled down to room temperature.

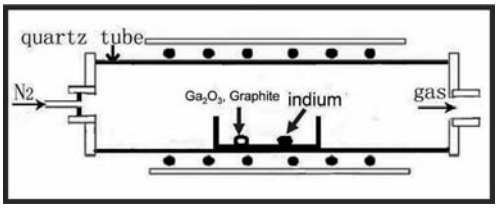

Figure 8. Schematic illustration of the CVD system for the synthesis of low-density, cone-like In_2O_3 NW arrays at 900 °C for 1 h.

When the mixture of gallium oxide and graphite and high-purity N_2 were replaced by a trace amount of oxygen (2 ppm) and industrial purity argon (purity 99.998%), respectively, and other reaction conditions were kept constant, high-density, cone-like In_2O_3 NW arrays were obtained on the surface of the indium grains. Here, the industrial purity argon serves not only as the oxygen source but also as carrier gas for the formation of In_2O_3 on the surface of the indium grains.

The as-synthesized products were characterized by X-ray powder diffraction (XRD) by using a SHIMADZU XRD-6000 diffractometer with Cu-K_α radiation (λ = 1.54056 Å) at 40 kV and 50 mA. Field emission scanning electron microscopy (FE-SEM) images were obtained with a JEOL S-4800 field emission microscope operating at an acceleration voltage of 10.0 kV. Transmission electron microscopy (TEM) images were captured with a JEOL JEM-2010 transmission electron microscope. Raman spectra were measured by using a Raman Microscope (RENISHAW, Britain) at room temperature. The 532.1 nm line from an Ar^+ laser was used as the incident light. Photoluminescence (PL) spectra were examined by using a fluorescence spectrophotometer (Edinburgh FLS920) with a Xe lamp at room temperature.

Acknowledgments

This work was supported by the National Natural Science Foundation of China (NSFC, Nos. 20731002, 10876002, 20871016, 20771022, 91022006, and 20973023), the 111 Project (B07012), the Program for New Century Excellent Talents in University, the Open Fund of State Key Laboratory of Explosion Science and Technology, and the Beijing Institute of Technology (Nos. ZDKT08-01 and YBKT09-13), the Specialized Research Fund for the Doctoral Program of Higher Education (SRFDP, No. 200800070015), the Funding Project for Science and Technology Program of Beijing Municipal Commission (No. Z09010300820902), and the Key Foundation of China Academy of Engineering Physics (No. 2009A0302017).

[1] Y. N. Xia, P. D. Yang, Y. G. Sun, Y. Y. Wu, B. Mayers, B. Gates, Y. D. Yin, F. Kim, Y. Q. Yan, *Adv. Mater.* **2003**, *15*, 353.
[2] H. J. Fan, P. Werner, M. Zacharias, *Small* **2006**, *2*, 700.
[3] C. Li, D. H. Zhang, S. Han, X. L. Liu, T. Tang, C. W. Zhou, *Adv. Mater.* **2003**, *15*, 143.
[4] X. Duan, Y. Huang, Y. Cui, J. Wang, C. M. Lieber, *Nature* **2001**, *409*, 66.
[5] M. H. Huang, S. Mao, H. Feick, H. Yan, Y. Wu, H. Kind, E. Weber, R. Russo, P. Yang, *Science* **2001**, *292*, 1897.
[6] J. Wang, M. S. Gudiksen, X. Duan, Y. Cui, C. M. Lieber, *Science* **2001**, *293*, 1455.
[7] Y. Cui, C. M. Lieber, *Science* **2001**, *291*, 851.
[8] M. Arnold, P. Avouris, Z. W. Pan, Z. L. Wang, *J. Phys. Chem. B* **2003**, *107*, 659.
[9] Q. Wan, E. N. Dattoli, W. Y. Fung, W. Guo, Y. B. Chen, X. Q. Pan, W. Lu, *Nano Lett.* **2006**, *6*, 2909.
[10] J. Goldberger, A. I. Hochbaum, R. Fan, P. D. Yang, *Nano Lett.* **2006**, *6*, 973.
[11] V. Schmidt, H. Riel, S. Senz, S. Karg, W. Riess, U. Gosele, *Small* **2006**, *2*, 85.
[12] K. G. Gopchandran, B. Joseph, J. T. Abaham, P. Koshy, V. K. Vaidyan, *Vacuum* **1997**, *48*, 547.
[13] S. T. Jean, Y. C. Her, *Cryst. Growth Des.* **2010**, *10*, 2104.
[14] B. X. Li, Y. Xie, M. Jing, G. X. Rong, Y. C. Tang, G. Z. Zhang, *Langmuir* **2006**, *22*, 9380.
[15] D. H. Zhang, C. Li, S. Han, X. L. Liu, T. Tang, W. Jin, C. W. Zhou, *Appl. Phys. Lett.* **2003**, *82*, 112.
[16] W. Y. Yin, M. H. Cao, S. J. Luo, C. W. Hu, B. Q. Wei, *Cryst. Growth Des.* **2009**, *9*, 2173.
[17] S. C. Chang, M. H. Huang, *J. Phys. Chem. C* **2008**, *112*, 2304.
[18] M. J. Zheng, L. D. Zhang, G. H. Li, X. Y. Zhang, X. F. Wang, *Appl. Phys. Lett.* **2001**, *79*, 839.
[19] P. Nguyen, H. T. Ng, T. Yamada, M. K. Smith, J. Li, J. Han, M. Meyyappan, *Nano Lett.* **2004**, *4*, 651.
[20] Q. Wan, M. Wei, D. Zhi, *Adv. Mater.* **2006**, *18*, 234.

[21] H. W. Kim, N. H. Kim, C. Lee, *Appl. Phys. A* **2005**, *81*, 1135.
[22] H. F. Yang, Q. H. Shi, B. Z. Tian, Q. Y. Lu, F. Gao, S. H. Xie, J. Fan, C. Z. Yu, B. Tu, D. Y. Zhao, *J. Am. Chem. Soc.* **2003**, *125*, 4724.
[23] C. Y. Wang, Y. Dai, J. Pezoldt, B. Lu, T. Kups, V. Cimalla, O. Ambacher, *Cryst. Growth Des.* **2008**, *8*, 1257.
[24] W. B. White, V. G. Keramidas, *Spectrochim. Acta A* **1972**, *28*, 501.
[25] E. Sutter, P. Sutter, *Nano Lett.* **2008**, *8*, 411.
[26] Z. W. Pan, Z. R. Dai, Z. L. Wang, *Science* **2001**, *291*, 1947.
[27] Q. Y. Zhang, K. M. Xu, *Indium Chemistry Handbook*, Peking University Press, Beijing, China, **2005**, p. 23.
[28] Y. Tian, Z. Hu, Y. Yang, X. Wang, X. Chen, H. Xu, Q. Wu, W. Ji, Y. Chen, *J. Am. Chem. Soc.* **2004**, *126*, 1180.
[29] H. Chen, Y. Yang, Z. Hu, K. Huo, Y. Ma, Y. Chen, X. Wang, Y. Lu, *J. Phys. Chem. B* **2006**, *110*, 16422.
[30] S. Hofman, G. Csányi, A. C. Ferrari, M. C. Payne, J. Robertson, *Phys. Rev. Lett.* **2005**, *95*, 036101.
[31] Z. L. Wang, *J. Phys. Chem. B* **2000**, *104*, 1153.
[32] H. B. Liu, X. C. Wu, L. F. Chi, D. Y. Zhong, Q. Zhao, Y. L. Li, D. P. Yu, H. Fuchs, D. B. Zhu, *J. Phys. Chem. C* **2008**, *112*, 17625.
[33] N. Liu, Q. Wu, C. Y. He, H. S. Tao, X. Z. Wang, W. Lei, Z. Hu, *ACS Appl. Mater. Interfaces* **2009**, *1*, 1927.
[34] J.-M. Bonard, K. A. Dean, B. F. Coll, C. Klinke, *Phys. Rev. Lett.* **2002**, *89*, 602.
[35] L. Nilsson, O. Groening, C. Emmenegger, O. Kuettel, E. Schaller, L. Schlapbach, H. Kind, J.-M. Bonard, K. Kern, *Appl. Phys. Lett.* **2000**, *76*, 2071.

Received: October 8, 2010
Published Online: February 15, 2011

